PROCEEDINGS, 51st Workshop on Geothermal Reservoir Engineering
Stanford University, Stanford, California, February 9-11, 2026
SGP-TR-230

Application of Deep Neural Operators for Thermal Response Test Analysis: A Data-Driven Approach for Ground Heat Exchanger Characterization

Nguyen T. Le[1,*], Aggrey Mwesigye[1], Philip Adebayo[1], and Roman Shor[2]

[1]University of Calgary, 2500 University Dr NW, Calgary, AB T2N 1N4, Canada

[2]Texas A&M University, 400 Bizzell St, College Station, TX 77843, USA

[*]nguyen.le@ualberta.ca

Keywords: deep neural operator, thermal response test, ground heat exchanger

ABSTRACT

Thermal response tests are essential for determining ground thermal properties required for optimal design of ground heat exchanger systems in shallow geothermal applications. This paper presents a novel Multiple-Input Deep Neural Operator variant for rapid and accurate thermal response test analysis across standard, constant temperature, and oscillatory protocols. The approach directly maps heat injection and fluid temperature time series to soil thermal conductivity, borehole thermal resistance, and (for the oscillatory case) soil volumetric heat capacity, without requiring iterative optimization. Models trained on synthetic samples generated by simulations generalize to six real-world datasets from Canada, Denmark, Japan, and the United States. For two-parameter inversion, mean absolute percentage errors are 4.98% for soil thermal conductivity and 2.75% for borehole thermal resistance. In the three-parameter oscillatory case, errors are 0.58% and 5.79% for the same parameters and 9.33% for soil volumetric heat capacity. The models cut interpretation time to seconds and generalize across different input functions without retraining, making it particularly valuable for rapid site assessment and ground-source heat pump system optimization. Future extensions include noise augmentation and physics-informed training.

1. INTRODUCTION

Ground-source heat pumps (GSHPs) represent a proven low-carbon technology for building heating and cooling by harnessing stable subsurface temperatures. In vertical configurations common on space-constrained sites, ground heat exchangers (GHEs) in boreholes extend tens to hundreds of meters deep to access a consistent geothermal resource, thereby minimizing seasonal fluctuations. Optimal GSHP deployment requires precise site-specific characterization of subsurface thermal properties, including soil thermal conductivity, soil volumetric heat capacity, and borehole thermal resistance (which is influenced by grout, pipe configuration, and geometry). Inaccurate estimates lead to oversized or underperforming fields, elevating upfront drilling costs, and risking long-term soil thermal imbalance from underbalanced heating/cooling loads (Fry et al., 2023). Thermal response tests (TRTs) have become the standard in-situ characterization technique because they provide a cost-effective alternative to core sampling and laboratory analysis, and are routinely analyzed based on simplified analytical models such as line source and cylindrical source formulations under constant heat injection conditions. However, modern practice increasingly employs variants such as constant-temperature TRTs and oscillatory TRTs to improve design flexibility and probe an additional parameter, which substantially complicates data interpretation due to time dependent boundary conditions, stronger parameter coupling, and the need to account for both injection and recovery phases.

In parallel, advances in scientific machine learning have created new opportunities to learn mappings between function spaces via neural operators, enabling data-driven surrogates for parametric partial differential equation (PDE) models that can directly operate on input and output fields rather than on hand-crafted features (Kovachki et al., 2023). Architectures such as Deep Operator Network (DeepONet) and its extensions, including Multi-Input Operator Network (MIONet), have demonstrated strong approximation capabilities and generalization across diverse operator learning tasks (Lu et al., 2019; Jin et al., 2022). These advancements enable operator surrogates for forward PDE solutions, but TRT inverse problems, mapping measurements back to parameters, typically retain iterative optimizer coupled to forward models.

This work proposes a novel inverse-operator framework for TRT interpretation in which a GRU-based MIONet learns the direct mapping from heat injection and fluid temperature time series, together with selected scalar descriptors, to key thermal parameters without requiring an external optimizer. By training a synthetic dataset generated using GHEtool and literature-based parameter ranges, the two proposed neural operator models tackle two-parameter inversion (soil thermal conductivity and borehole thermal resistance) in standard and constant-temperature TRTs, alongside three-parameter inversion (including soil volumetric heat capacity) in oscillatory TRTs. Applied to six real-world TRT datasets from different operational settings across Canada, Denmark, Japan, and the United States, the approach aims to demonstrate that neural operators can achieve field-relevant accuracy, handle heterogeneous test protocols, and provide a flexible foundation for future extensions such as physics-informed training and real-time TRT analysis.

2. BACKGROUND

2.1 Thermal Response Test

GSHPs use the ground as a stable temperature heat source in winter and a heat sink in summer. GHEs serve as the interface between the ground-coupled heat pump (GCHP) systems, a subset of GSHP also known as a closed-loop heat pump, and the surrounding soil or rock.

In vertical closed-loop systems, one or more boreholes are drilled to depths of a few tens to several hundred meters, and polyethylene U-tubes or coaxial pipes are installed and backfilled with thermally conductive grout to ensure optimal thermal contact and groundwater protection (Sarbu and Sebarchievici, 2014). A circulating fluid transfers heat rejected from the building in cooling mode and the heat extracted from the ground in heating mode.

GHE performance depends mainly on ground thermal properties, borehole and pipe geometry, and grout thermal properties (Khaleghi and Livescu, 2023). Proper GHE design, therefore, requires reliable values of these site-specific thermal properties. TRTs provide a cost-effective means to determine these parameters, serving as an alternative to core sampling and core analysis (Reuss et al., 2009). TRTs involve injecting a controlled heat load into a test borehole while monitoring inlet and outlet fluid temperatures (Figure 1). Electrical input power, fluid temperatures, and flow rate are measured over time and recorded typically every 1–10 minutes.

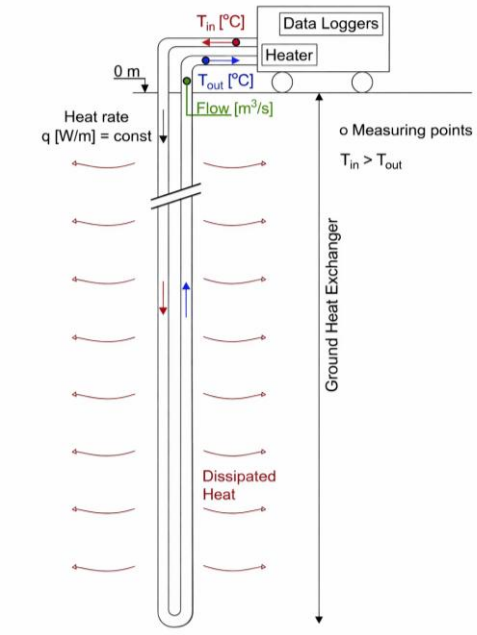

Figure 1. Schematic of standard TRT setup (Alberdi-Pagola et al., 2018).

In standard TRTs, heat is injected at a constant rate for 48–72 hours. Input power is recommended to maintain a standard deviation below 1.5% and a maximum variation under 10% of the mean value (Javed and Fahlén, 2011). These strict power requirements enable the use of simplified analytical solutions, such as line-source and cylindrical-source models, to estimate ground thermal conductivity and borehole thermal resistance from TRT data. The recovery period, the phase where heat injection ceases but fluid circulation continues with temperature monitoring, is optional.

One variant of TRT, often called thermal performance test (TPT) or constant temperature thermal response test (CT-TRT), is where fluid temperature is held constant by adjusting heat injection rate using proportional-integral-derivative (PID)-controlled heaters. TPT data analysis, which involves Bayesian inference and Markov chain Monte Carlo of the temporal superposed form of an infinite line-source model (Choi et al., 2018), is significantly more complex than the standard TRT analysis.

Another variant of TRT, called oscillatory TRT (OTRT), applies a periodic heat injection function rather than constant power. This enables estimation of ground heat capacity alongside ground thermal conductivity and borehole thermal resistance. The analysis of OTRT data, however, involves additional steps of linear trend removal and oscillatory amplitude and phase analysis, and the recovery period is no longer optional (Giordano et al., 2021).

2.2 Neural Operator

Neural operators constitute a class of deep learning architectures designed to learn mappings between function spaces, unlike traditional neural networks, which operate on finite-dimensional vectors. This function-to-function approach offers two key advantages. First, it aligns naturally with the mathematical structure of scientific problems where inputs and outputs are functions, such as boundary conditions and the solution field of a boundary value problem. Second, it allows a single trained model to capture the full solution operator representing the intrinsic dynamics of a system and to accommodate input variations without retraining (Kovachki et al., 2023).

DeepONet is a prominent neural operator architecture that comprises two subnetworks: a branch net that encodes the input function by its values at sensor locations and a trunk net that encodes the output query location. In its standard unstacked form, DeepONet employs a single branch net for the input function and fully connected layers for both branch and trunk nets. DeepONet achieves lower test error, faster convergence, and better generalization compared to fully connected neural networks across various ordinary and partial differential equation examples (Lu et al., 2019).

MIONet extends DeepONet by incorporating multiple branch nets to handle multiple input functions. In its standard low rank configuration, the trunk output matches the dimension as each branch output and fully connected architecture is used for all branch nets and trunk net. This design enables efficient learning of multiple input operators and MIONet outperforms concatenated DeepONet across various examples (Jin et al., 2022).

3. METHODOLOGY

3.1 Overview

TRT analysis is fundamentally an inverse problem in which thermal properties are inferred from measured fluid temperature after applying a known heat injection at the borehole. The forward problem, where heat injection and thermal properties are given, and the temperature field is to be solved, has been studied extensively. Commonly used forward models (e.g., infinite line source, infinite cylindrical source, finite line source) represent different approximations of the same transient heat conduction initial-boundary value problems with a controlled boundary condition at the borehole. For example, the governing equation, boundary conditions, initial condition, and analytical solution for the infinite cylindrical source model (Carslaw and Jaeger, 1959) are shown in Equations 1–5.

$$\lambda_s\left(\frac{\partial^2 T_s}{\partial r^2}+\frac{1}{r}\frac{\partial T_s}{\partial r}\right)=c_s\frac{\partial T_s}{\partial t} \tag{1}$$

$$\lambda_s\frac{\partial T_s}{\partial r}\Big|_{r=r_b}=-\frac{q}{2\pi r_b} \tag{2}$$

$$T_s\big|_{r\to\infty}=T_{om} \tag{3}$$

$$T_s\big|_{t=0}=T_{om} \tag{4}$$

$$T_s=T_{om}+\frac{q}{\pi^2\lambda_s}\int_0^\infty\frac{Y_0(\eta z)J_1(z)-J_0(\eta z)Y_1(z)}{z^2[J_1^2(z)+Y_1^2(z)]}(1-e^{-z^2F_0})dz \tag{5}$$

In a TRT, the controllable aspect is the boundary condition at the borehole, for instance, a Neumann boundary in standard TRTs (Equation 2), a periodic boundary in oscillatory TRTs, and a Dirichlet boundary in TPTs. Even when the governing equation (1) remains the same, different borehole boundary conditions (2) lead to different solutions. The mapping from borehole boundary condition functions to solution functions can be learned by a neural operator which takes the heat injection function as input for the branch net, scalar parameters as input for the trunk net, and the fluid temperature function as output. Using this forward operator approach, however, will require an external optimizer to iteratively estimate the ground and borehole thermal properties (Figure 2, left).

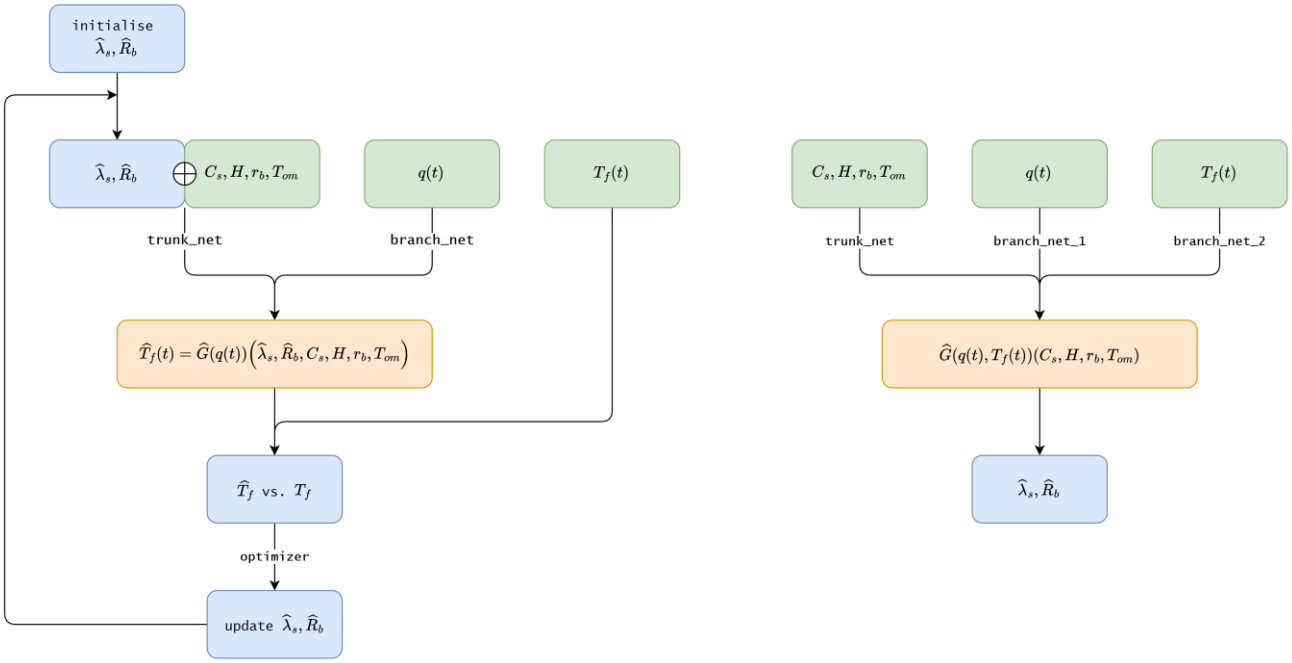

Figure 2. Forward operator with an optimizer (left) and inverse operator without an optimizer (right) in two-parameter inversion scenario; for three-parameter inversion, soil volumetric heat capacity is moved from trunk net input to output.

The inverse operator approach eliminates the need for this external optimizer. In this method, a neural operator takes heat injection and fluid temperature functions as inputs for branch nets and scalar parameters as input for the trunk net. The two input functions can be either concatenated and fed into a single branch net, or they can be fed separately into two branch nets (Figure 2, right). Although the former requires less memory, the latter provides a more systematic and flexible solution as each input function is treated independently. Therefore, this paper focuses on the use of MIONet for direct inversion without relying on an external optimizer. Specifically, two inversion scenarios involving two parameters (soil thermal conductivity and borehole thermal resistance) and three parameters (soil thermal conductivity, borehole thermal resistance, and soil volumetric heat capacity) are examined.

3.2 Training Data Generation

Generating training datasets first require soil and borehole thermal properties, including soil thermal conductivity, soil volumetric heat capacity, far-field temperature, borehole length, borehole radius, and borehole thermal resistance. These scalar parameters are uniformly sampled within the ranges reported in published literature (Table 1).

Table 1. Ranges of scalar parameters.

Parameters	Minimum	Maximum	Unit	Source
Soil thermal conductivity λ_s	1.5	3.5	W/(m.K)	Tarnawski et al., 2015
Soil volumetric heat capacity C_s	1.5e6	3.0e6	J/(m^3.K)	Kodešová et al., 2013
Far-field temperature T_{om}	5	25	C	Grasby et al., 2011
Borehole length H	10	160	m	Yang et al., 2010
Borehole radius r_b	0.075	0.225	m	Yang et al., 2010
Borehole thermal resistance R_b	0.05	0.25	m.K/W	Tarrad, 2021

Heat injection functions are generated as time series using truncated Chebyshev series (Equation 6) with coefficients a_k uniformly sampled within interval [-1, 1], maximum injection rate $q_{\max}$ and injection duration T uniformly sampled within common ranges of 25–175 W/m and 50–150 hours (Laloui and Loria, 2019), respectively (Figure 3, left and Figure 4, left).

$$q(t) = q_{\max} \sum_{k=0}^{T} a_k T_k(t) \tag{6}$$

Fluid temperature functions are obtained as time series using GHEtool, given combinations of scalar parameters and heat injection time series. This fluid temperature is computed from borehole wall temperature obtained by convolving the heat injection with appropriate g-functions (Peere and Blanke, 2022). For two-parameter inversion, recovery periods are trimmed, and the fluid temperature time series are zero-padded to 200 hours (Figure 3, right) while for three-parameter inversion, the recovery periods remain unaltered (Figure 4 right).

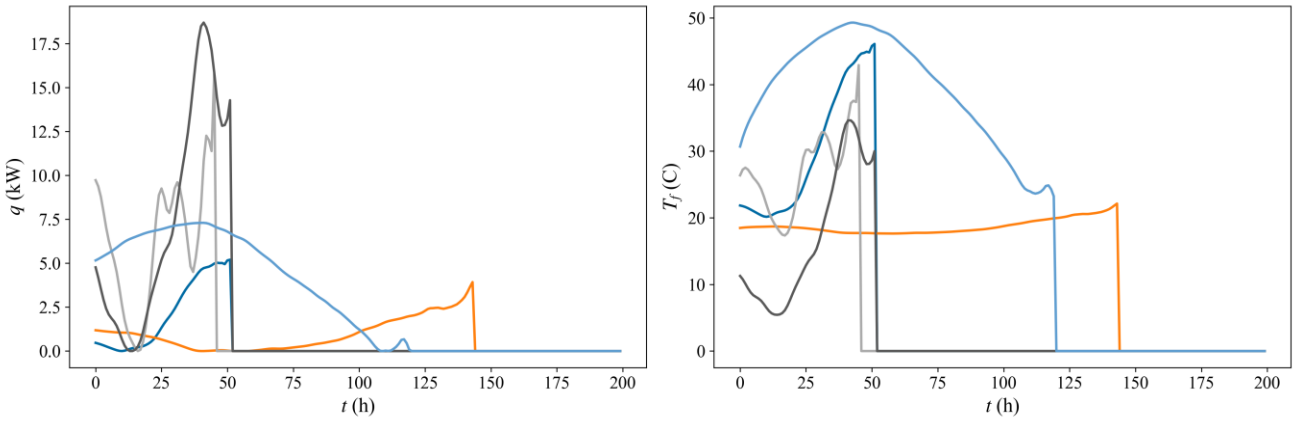

Figure 3. Examples of generated heat injection (left) and corresponding simulated fluid temperature (right) used for training for two-parameter inversion.

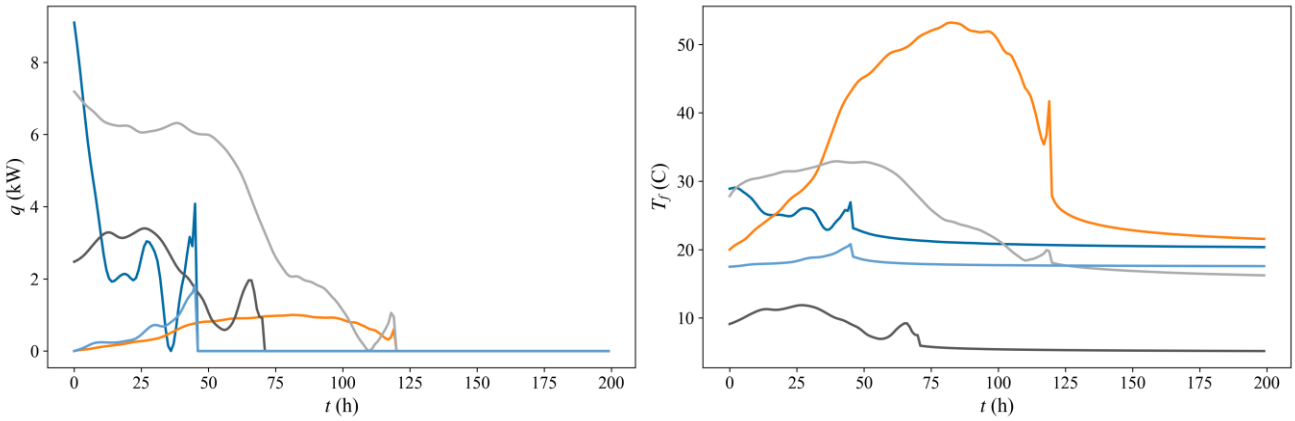

Figure 4. Examples of generated heat injection (left) and corresponding simulated fluid temperature (right) used for training for three-parameter inversion.

The training datasets consist of the Cartesian product of all scalar parameters and heat injection time series, along with their corresponding fluid temperature time series. Extreme combinations that cause GHEtool to produce missing values in the fluid temperature are pruned. After pruning, the total number of training combinations is approximately 6.5 million. Scalar parameters are divided into input for trunk net (C_s, T_{om}, H, r_b for two-parameter inversion and T_{om}, H, r_b for three-parameter inversion) and output (λ_s, R_b for two-parameter inversion and λ_s, C_s, R_b for three-parameter inversion). Heat injection and fluid temperature time series are packed into appropriate shapes to serve as inputs of respective branch nets separately.

3.3 Model Architecture and Training

As illustrated in Figure 2, we aim to approximate operator **G** that maps input functions q and T_f, along with input parameters x to output parameters y. The MIONet used in this study is the low-rank variant consisting of two independent branch nets, a trunk net, and an output merger net. The operator **G** can be regarded as a function of x conditioned on q and T_f (Equation 7).

$$\hat{\mathbf{G}}(q,T_f)(x) = \mathbf{h}\left(\mathbf{g}_1(q)\cdot\mathbf{g}_2(T_f)\cdot\mathbf{f}(x)\right) \tag{7}$$

Each data sample includes q, T_f, and x. Heat injection function q, represented discretely at m sensor locations (i.e., time steps) as [q_1, q_2, … q_m], is passed into branch net $\mathbf{g_1}$ to output $\mathbf{g_1}(q)$. Similarly, fluid temperature function T_f, given as [T_{f1}, T_{f2}, … T_{fm}], is fed into branch net $\mathbf{g_2}$ yielding $\mathbf{g_2}(T_f)$. The trunk net takes input x, which represents query locations. In the two-parameter inversion case, x is the vector [C_s, T_{om}, H, r_b, p] while in the three-parameter inversion case, it is [T_{om}, H, r_b, p] with p being an integer used to encode the position of the parameters to be inverted. The trunk net **f** processes x to generate **f**(x). Outputs of the two branch nets and the trunk net are combined through element-wise multiplication before being passed into the output merger net **h**. The output y of each data sample is either {λ_s, R_b} or {λ_s, C_s, R_b} depending on the number of parameters being inverted.

In this work, branch nets are based on Gated Recurrent Unit (GRU), a type of recurrent neural network architecture (Figure 5). The two branch nets are identical, each consisting of a stacked GRU network with five layers where each layer has a hidden size of 190. A fully connected layer with 190 neurons follows the GRU layers. This fully connected layer ensures that branch net outputs match the dimensions of trunk net output, as the element-wise product requires this alignment. The trunk net is a fully connected neural network with five layers, each containing 190 neurons. The output merger net is a two-layer fully connected neural network, with the first layer having 95 neurons and the second layer having one neuron. The GRUs in branch nets use standard GRU activation functions: sigmoid for update and reset gates, and tanh for candidate hidden state). The trunk net uses tanh as activation functions on all layers, while the output merger net uses sigmoid activation function. The same architecture is used for two-parameter inversion and three-parameter inversion cases.

The network is trained with 10 cycles of alternate Adam and L-BFGS optimizers. Each cycle begins with 5,000 iterations using Adam, then 20,000 iterations using L-BFGS, optimizing for mean square error (MSE) (Equation 8). The learning rate for Adam is set to 5e-5, while L-BFGS uses a history size of 100. Adams performs well during initial training phases with fast convergence through noisy loss landscape through adaptive momentum and first order gradients. L-BFGS, on the other hand, excels in fine tuning for precise minimization using second-order information (Lu et al., 2021). Therefore, alternating between Adam and L-BFGS accelerates reaching a minimum reliably. The training/validation split is 0.8/0.2 and the optimal iteration is selected based on validation loss.

$$MSE = \frac{1}{N}\sum_{i=0}^{N}(y_i - \hat{y}_i)^2 \tag{8}$$

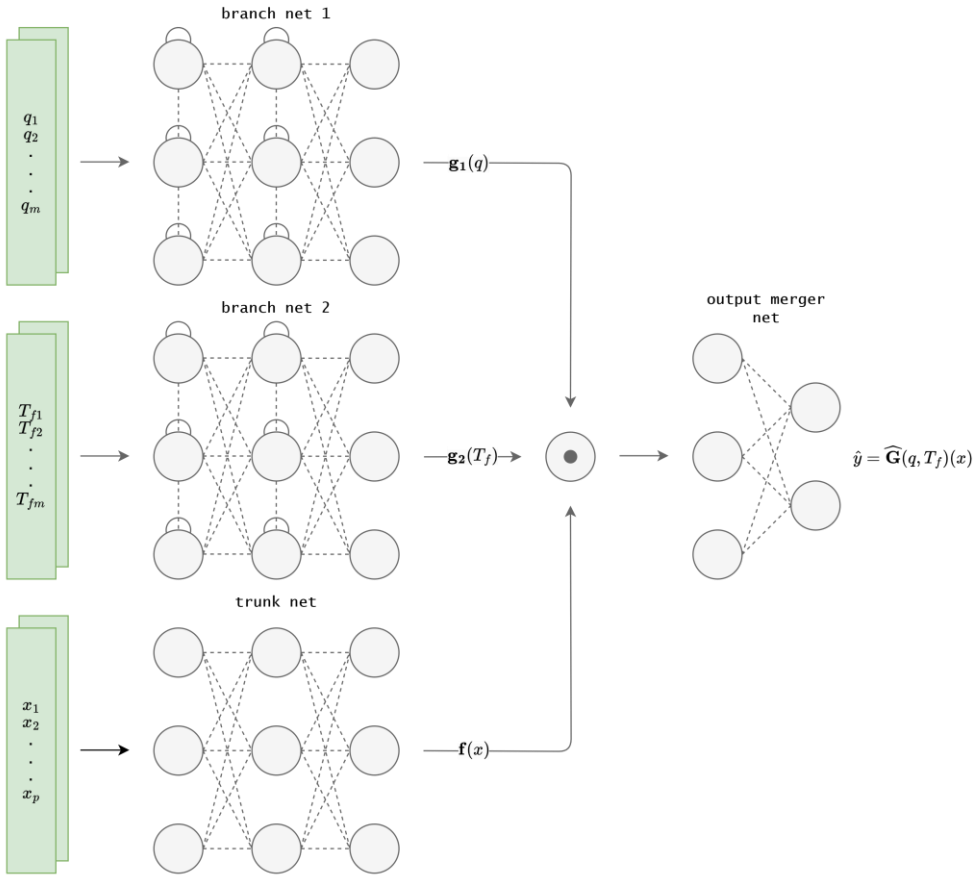

Figure 5. Schematic of the MIONet variant used in this work.

4. RESULTS

The test set consists of six real-world datasets with their corresponding sources, inversed parameters, test types, and test locations detailed in Table 2.

Table 2. Metadata of test datasets.

Test	Test type	Inversed parameters	Location	Source
1	Standard	λ_s, R_b	Denmark	Alberdi-Pagola et al., 2018
2	Standard	λ_s, R_b	United States	Beier et al., 2011
3	Standard	λ_s, R_b	Canada	This paper
4	Performance	λ_s, R_b	Japan	Choi et al., 2018
5	Performance	λ_s, R_b	Japan	Choi et al., 2018
6	Oscillatory	λ_s, R_b, C_s	Canada	Giordano et al., 2021

All datasets are preprocessed to ensure consistent format. The heat injection and fluid temperature measurements are resampled to an hourly resolution. For both two-parameter and three-parameter inversions, heat injection data are zero-padded to a total length of 200 hours (Figure 6, left; Figure 7, left). Fluid temperature data, however, require different padding approaches because the recovery period is of varying importance and availability across inversion types. In the case of two-parameter inversion, the recovery period is not critical for inversion process and is not consistently available across all datasets; therefore, fluid temperature data are zero-padded to a length of 200 (Figure 6, right). For three-parameter inversion, the recovery period plays a key role and must be included in fluid temperature record (Figure 7, right). To eliminate the near-borehole effect, the first 10 hours of both heat injection and fluid temperature data are trimmed,

resulting in a dimension of 190 for each. Finally, scalar input parameters are assembled into a vector following the same sequence described in Subsection 3.3.

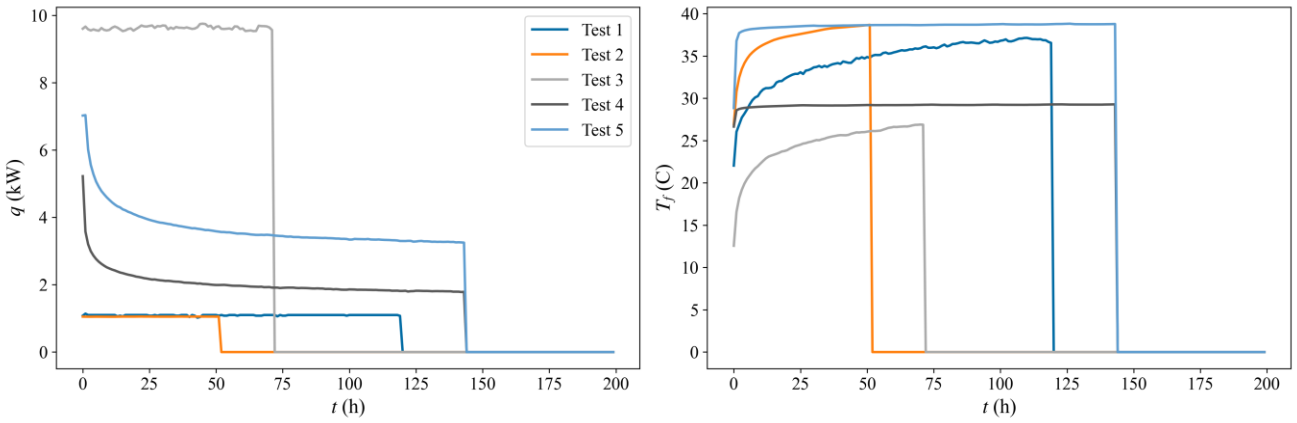

Figure 6. Heat injection and fluid temperature of Tests 1–5.

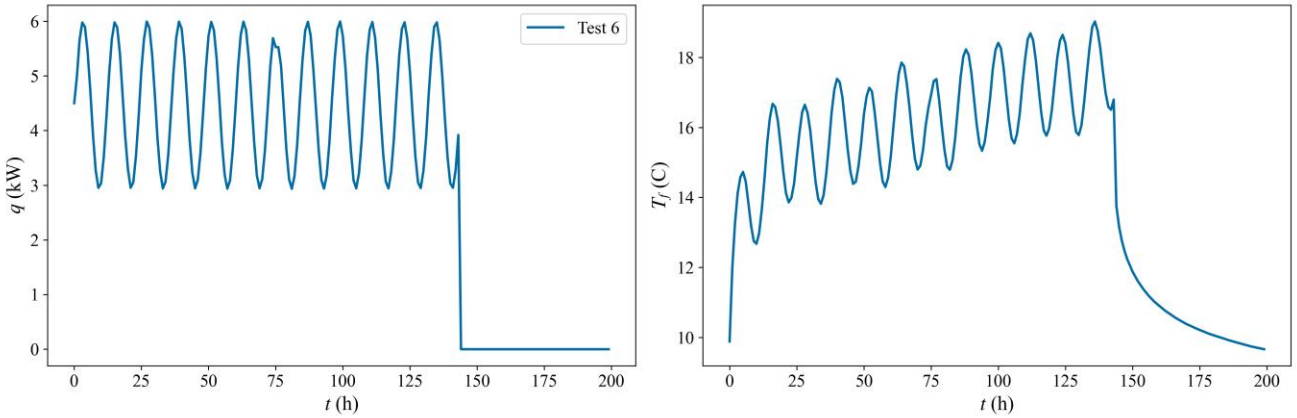

Figure 7. Heat injection and fluid temperature of Test 6.

The model predictions are evaluated against the corresponding true values listed in Table 2 using mean absolute percentage error (MAPE) defined in Equation 9. The predicted values and the true values alongside their uncertainty ranges for λ_s and R_b are visualized in Figure 8.

$$MAPE = \frac{100}{N}\sum_{i=0}^{N}\left|\frac{y_i - \hat{y}_i}{y_i}\right| \tag{9}$$

Table 2. Test set labels, predictions, and absolute percentage errors.

Test	True λ_s	Predicted λ_s	Error	True R_b	Predicted R_b	Error	True C_s	Predicted C_s	Error
1	2.30	2.40	4.15%	0.174	0.177	1.54%			
2	2.82	3.01	6.81%	0.173	0.174	0.39%			
3	2.08	2.19	5.51%	0.149	0.153	2.53%			
4	1.86	1.97	6.18%	0.140	0.152	8.40%			
5	1.92	1.88	2.24%	0.137	0.138	0.87%			
6	1.74	1.73	0.58%	0.081	0.086	5.79%	1.80e6	1.96e6	9.33%

For the two-parameter inversion cases (Tests 1–5), the overall MAPE is 4.98% for λ_s and 2.75% for R_b, indicating good predictive performance. The individual test results show consistent performance with λ_s errors ranging from 2.24% to 6.81%, and R_b errors ranging from 0.39% to 8.40%. Notably, the model performs well across different test types, successfully handling standard TRTs as well as TPTs.

The three-parameter inversion case (Test 6) presents a more complex scenario as it requires estimation of an additional parameter, the volumetric heat capacity C_s. For this test, the model achieves particularly good accuracy for λ_s with an error of only 0.58%, suggesting that the inclusion of recovery period data significantly improves thermal conductivity estimation. The error for R_b is 5.79%, which remains within acceptable bounds and is consistent with the performance observed in two-parameter inversion cases. However, the error C_s is notably high at 9.33%, reflecting inherent challenges in estimating soil heat capacity from OTRTs where parameter sensitivity and coupling effects can complicate the inversion process.

The visualization of uncertainty ranges alongside predicted values provides additional insight into model reliability (Figure 8). For both λ_s and R_b, predicted values consistently fall within or close to the true uncertainty ranges across all tests.

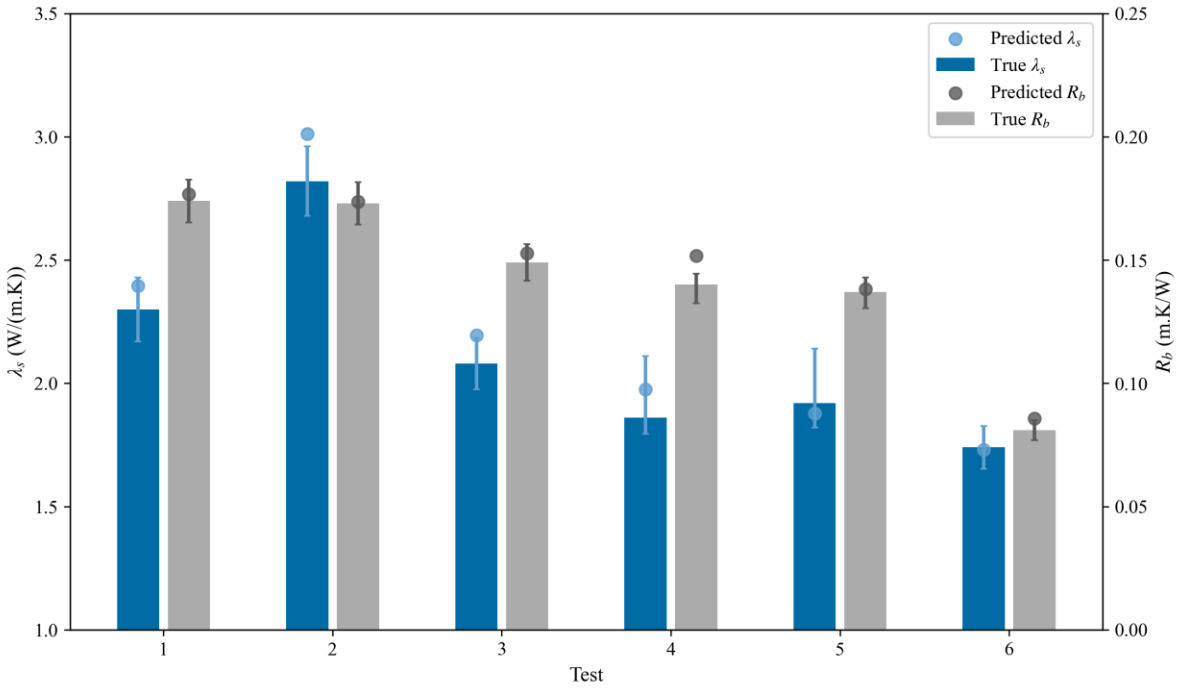

Figure 8. True values with corresponding uncertainty ranges and predicted values of soil thermal conductivity and borehole thermal resistance (uncertainty ranges for Test 2 were not reported, the whiskers represent 5%).

5. CONCLUSIONS

This paper presents a novel variant of the MIONet that incorporates GRU-based branch nets for inverse analysis of TRT data. This architecture enables direct estimation of soil thermal conductivity and borehole thermal resistance from heat injection and fluid temperature time series, bypassing the need for external optimization. The model exhibits robust generalization across diverse TRT variants, including standard TRTs and TPTs, delivering consistent predictive accuracy on real-world datasets. Challenges remain in accurately estimating soil volumetric heat capacity using OTRT data.

The proposed MIONet achieves MAPEs of 4.98% and 2.75% for soil thermal conductivity and borehole thermal resistance, respectively, across five real-world tests spanning standard TRTs and TPTs. Model predictions consistently align with or fall close to reported uncertainty ranges confirming model's robustness without needing an external optimizer. For three-parameter inversion including soil volumetric heat capacity, the model handles OTRT data effectively for soil thermal conductivity (0.58% error) and borehole thermal resistance (5.79% error). Estimating soil volumetric heat capacity proves challenging, yielding a 9.33% MAPE in the case of three-parameter inversion using OTRT data. Data preprocessing which involves resampling of heat injection and fluid temperature may introduce minor artifacts what amplify errors in complex inversions.

Future work could incorporate physics-informed losses to improve heat capacity estimations. Model extensions to different borehole types or real-time deployment would broaden applicability. Training on diverse, noise-augmented synthetic datasets mirroring field conditions could improve generalizability. Additionally, investigating cases with errors exceeding 5% could reveal some clues to model architecture refinements.

NOMENCLATURE

.	Element-wise product
^	Estimate
α_s	Soil thermal diffusivity
η	Dimensionless radial coordinate
λ_s	Soil thermal conductivity
a_k	Chebyshev coefficient
C_s	Soil volumetric heat capacity
F_0	Fourier number
f	Trunk net
G	Operator
g	Branch net
H	Borehole length
h	Output merger net
J_0	Bessel function of first kind, order 0
J_1	Bessel function of first kind, order 1
m	Branch net input dimension
N	Number of data samples
q	Heat injection rate
$q_{\max}$	Maximum heat injection rate
r	Radial coordinate
r_b	Borehole radius
R_b	Borehole thermal resistance
T	Injection duration
t	Temporal coordinate
T_f	Fluid temperature
T_k	Chebyshev polynomial of first kind
T_{om}	Far-field temperature
x	Trunk net input
Y_0	Bessel function of second kind, order 0
Y_1	Bessel function of second kind, order 1
y	Operator output

ACKNOWLEDGMENTS

The first author extends sincere gratitude to Viridien Group for facilitating the conditions that made this research possible.

REFERENCES

Alberdi-Pagola, M., Poulsen, S.E., Loveridge, F., Madsen, S., and Jensen, R.L.: Comparing Heat Flow Models for Interpretation of Precast Quadratic Pile Heat Exchanger Thermal Response Tests, Energy, 145, (2018), 721-733.

Beier, R.A., Smith, M.D., and Spitler, J.D.: Reference Data Sets for Vertical Borehole Ground Heat Exchanger Models and Thermal Response Test Analysis, Geothermics, 40(1), (2011), 79-85.

Carslaw, H.S., and Jaeger, J.C.: Conduction of Heat in Solids, 2nd ed., (1959).

Choi, W., Kikumoto, H., and Ooka, R.: New Perspectives in Thermal Performance Test: Cost-Effective Apparatus and Extended Data Analysis, Energy and Buildings, 180, (2018), 109-121.

Fry, N., Adebayo, P., Tian, R., Shor, R., and Mwesigye, A.: Underground Thermal Energy Storage at Scale: A Review of Techniques and a Case Study for Calgary, Alberta, Proceedings, 2023 Geothermal Rising Conference: Using the Earth to Save the Earth (GRC 2023), Geothermal Resources Council, (2023), 2157–2184.

Grasby, S.E., Jessop, A., Kelman, M., Ko, M., Chen, Z., Allen, D.M., Bell, S., Ferguson, G., Majorowicz, J., Moore, M., and Raymond, J.: Geothermal Energy Resource Potential of Canada, (2011).

Javed, S., and Fahlén, P.: Thermal Response Testing of a Multiple Borehole Ground Heat Exchanger, International Journal of Low-Carbon Technologies, 6(2), (2011), 141-148.

Jin, P., Meng, S., and Lu, L.: MIONet: Learning Multiple-Input Operators via Tensor Product, SIAM Journal on Scientific Computing, 44(6), (2022), A3490–A3514.

Khaleghi, K., and Livescu, S.: A Review of Vertical Closed-Loop Geothermal Heating and Cooling Systems with an Emphasis on the Importance of the Subsurface, Journal of Petroleum Science and Engineering, 220, (2023), 111137.

Kodešová, R., Vlasáková, M., Fér, M., Teplá, D., Jakšík, O., Neuberger, P., and Adamovský, R.: Thermal Properties of Representative Soils of the Czech Republic, (2013), 141-150.

Kovachki, N., Li, Z., Liu, B., Azizzadenesheli, K., Bhattacharya, K., Stuart, A., and Anandkumar, A.: Neural Operator: Learning Maps Between Function Spaces with Applications to PDEs, Journal of Machine Learning Research, 24(89), (2023), 1–97.

Laloui, L., and Rotta Loria, A.F.: Analysis and Design of Energy Geostructures: Theoretical Essentials and Practical Application, Academic Press, (2019), 821-932.

Lu, L., Jin, P., and Karniadakis, G.E.: DeepONet: Learning Nonlinear Operators for Identifying Differential Equations Based on the Universal Approximation Theorem of Operators, arXiv preprint arXiv:1910.03193, (2019).

Lu, L., Meng, X., Mao, Z., and Karniadakis, G.E.: DeepXDE: A Deep Learning Library for Solving Differential Equations, SIAM Review, 63(1), (2021), 208–228.

Peere, W., and Blanke, T.: GHEtool: An Open-Source Tool for Borefield Sizing in Python, Journal of Open Source Software, 7(76), (2022), 4406.

Reuss, M., Proell, M., and Nordell, B.: IEA ECES-Annex 21: Thermal Response Test, Proceedings, International Conference on Thermal Energy Storage, 14–17 June 2009, Energi-och Miljötekniska Föreningen/EMTF Förlag, (2009).

Sarbu, I., and Sebarchievici, C.: General Review of Ground-Source Heat Pump Systems for Heating and Cooling of Buildings, Energy and Buildings, 70, (2014), 441-454.

Tarnawski, V.R., Momose, T., McCombie, M.L., and Leong, W.H.: Canadian Field Soils III. Thermal-Conductivity Data and Modeling, International Journal of Thermophysics, 36(1), (2015), 119-156.

Tarrad, A.H.: Borehole Thermal Analysis for a Closed Loop Vertical U-Tube DX Ground Heat Exchanger, Mathematical Modelling of Engineering Problems, 8(4), (2021), 501-509.

Yang, H., Cui, P., and Fang, Z.: Vertical-Borehole Ground-Coupled Heat Pumps: A Review of Models and Systems, Applied Energy, 87(1), (2010), 16-27.